



Journal of Mining and Environment (JME)
journal homepage: www.jme.shahroodut.ac.ir



Delineation of Alteration Zones Based on Wavelet Neural Network (WNN) and Concentration–Volume (C-V) Fractal Methods in the Hypogene Zone of Porphyry Copper Deposit, Shahr-e-Babak District, SE Iran

Bashir Shokouh Saljoughi* and Ardeshir Hezarkhani

Department of Mining and Metallurgy Engineering, Amirkabir University of technology, Tehran, Iran

Article Info

Received 18 September 2020

Received in Revised form 8 October 2020

Accepted 10 October 2020

Published online 8 November 2020

DOI: [10.22044/jme.2020.10079.1944](https://doi.org/10.22044/jme.2020.10079.1944)

Keywords

Alteration zones

Ordinary Kriging (OK)

C-V fractal model

Wavelet

Wavelet Neural Network (WNN)

Abstract

In this paper, we aim to achieve two specific objectives. The first one is to examine the applicability of wavelet neural network (WNN) technique in ore grade estimation, which is based on integration between wavelet theory and Artificial Neural Network (ANN). Different wavelets are applied as activation functions to estimate Cu grade of borehole data in the hypogene zone of porphyry ore deposit, Shahr-e-Babak district, SE Iran. WNN parameters such as dilation and translation are fixed and only the weights of the network are optimized during its learning process. The efficacy of this type of network in function learning and estimation is compared with Ordinary Kriging (OK). Secondly, we aim to delineate the potassic and phyllic alteration regions in the hypogene zone of Cu porphyry deposit based on the estimation obtained of WNN and OK methods, and utilize Concentration-Volume (C-V) fractal model. In this regard, at first C-V log-log plots are generated based on the results of OK and WNN. The plots then are used to determine the Cu threshold values of the alteration zones. To investigate the correlation between geological model and C-V fractal results, the log ratio matrix is applied. The results showed that, Cu values less than 1.1% from WNN have more overlapped voxels with phyllic alteration zone by overall accuracy (OA) of 0.74. Spatial correlation between the potassic alteration zones resulted from 3D geological modeling and high concentration zones in C-V fractal model showed that the alteration zone has Cu values between 1.1% and 2.2% with OA of 0.72 and finally have an appropriate overlap with Cu values greater than 2.2% with OA of 0.7. Generally, the results showed that the WNN (Morlet activation function) with OA greater than OK can be a suitable and robust tool for quantitative modeling of alteration zones, instead of qualitative methods.

1. Introduction

The lateral and vertical grade variability is affected by various factors including rock type and alteration variations [1, 2]. Therefore, delineating the different alteration patterns and investigating their spatial variability are important tasks for mining engineers and geologists and play a significant role in grade distribution within porphyry ore deposits [3, 4]. In the recent decades, several methods and techniques have been utilized to delineate alteration zones in hydrothermal deposits. Some of these methods include: (1) geological investigations based on the

mineralogical and petrographical assemblages of minerals, (2) geochemical methods based on the thin sections, X-Ray Diffraction (XRD), Electron Probe Micro Analyzer (EPMA), Scanning Electron Microscopy (SEM) and Portable Infrared Mineral Analyzer (PIMA), (3) based on the studies of fluid inclusions in the porphyry deposits and, (4) based on the investigation of the isotope value variations in different zones of the porphyry deposits [5-12].

Despite the great functionality and excellent efficiency of the mentioned methods, ore grade variability has not been considered widely, even

✉ Corresponding author: bashir.shokouh@gmail.com (B. Shokouh Saljoughi).

though, as a significant matter, the porphyry deposits have shown zonation based on the grade variations in the ore elements [4, 13]. On the other hands, taking the ore element grade values into account will lead to a better geological interpretation of the delineation alteration patterns and the spatial variability of them. According to the high importance of the grade in the quantitative modeling, the choice of the appropriate estimation method is very critical as the methods including fractal and multi-fractal and, especially the C–V modeling depend on the concentration [14]. In the last three decades, several methods such as geostatistical [15–17], fractal and multi-fractal [13] [18– 26] and, different types of ANNs techniques [27–32] have been used in modeling the spatial variability and distributions of the uncertain surveyed data.

In this paper, wavelet neural network (WNN) combining the properties of the wavelet transform and the advantages of ANNs and Ordinary Kriging (OK) are applied to estimate cu grade in a hypogene zone. After the comparison of obtained results, WNN and C-V fractal modeling are used to

delineate the alteration regions in the hypogene zone of the porphyry ore deposit in Shahr-e-Babak district, SE of Iran.

2. Study area

There are many structural and lithotectonic zones in Iran [33] that generally are divided into the following categories: i) Zagros, ii) Sanandaj-Sirjan, iii) Sahand-Bazman, iv) Central Iran, v) Alborz, vi) Kope Dag, vii) Lut block, viii) Makran, and, ix) the East- Iranian suture zone. The Urumieh-Dokhtar Magmatic orogenic zone which formed as a result of subduction of the Arabian plate beneath central Iran during the Alpine orogeny, hosts all known Iranian porphyry copper mineralizations (**Figure 1**) such as Sar-Cheshmeh and Sungun deposits [33]. The study area is positioned in 45 km NE of the Shahr-Babak area and 85 km NW of the Sar Cheshmeh porphyry copper deposit in Kerman province, Iran (**Figure 1**). This deposit is located at latitudes $30^{\circ}10' 27''$ and $29^{\circ} 56' 55''$ N, and longitudes $55^{\circ} 10' 8''$ and $55^{\circ} 52' 28''$ E [34].

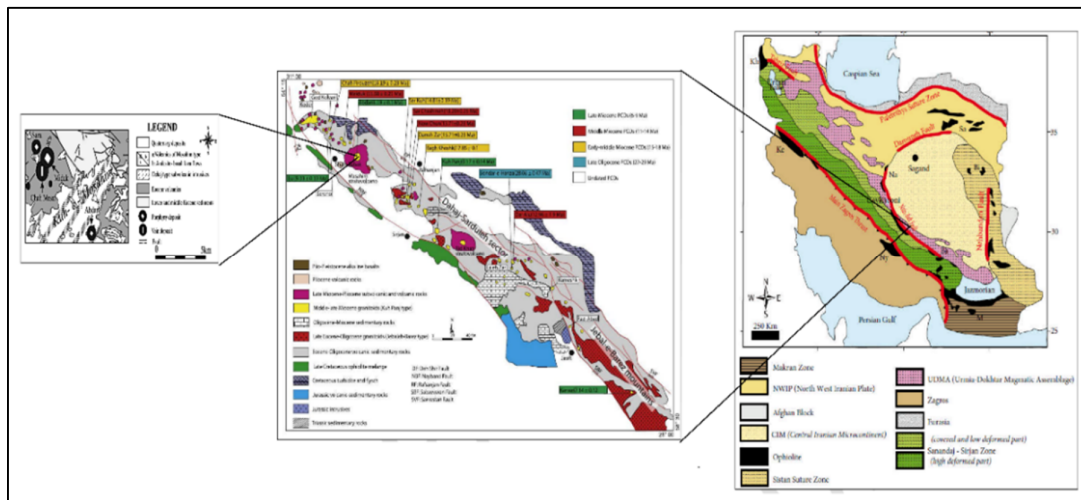


Figure1. The structural and geological map of the case study in the Shahr-e-Babak district, SE Iran.

It is a quartz diorite-related deposit. Ore in case study is fungi-form with 350×400 m dimensions and its upper part consists of oxide-zone and supergene-zone (mostly chalcocite). The Razak volcanic complex is the main host rock of the deposit [34]. The complex is divided into three main units: (i) lower part mainly consist of mafic sub-complex (trachybasalt, andesite and trachyandesite); (ii) a middle felsic sub-complex (tuff); and (iii) an upper mafic sub-complex (trachyandesite and andesite– basalt). The oldest units in the area (**Figure 1**) are Cenomanian –

Turonian calcareous flysch that covered by Eocene flysch. From bottom to top the porphyry system comprises three distinct Cu reservoirs: (1) the hypogene zone contains primary high-temperature sulfides (mixtures of chalcopyrite and pyrite) and disseminated blebs of magnetite and anhydrite. The occurrence of quartz–chalcopyrite–pyrite veins and veinlets indicates intense stockwork mineralization in the potassic zone. Pyrite is the most abundant hypogene sulfide in sericitic alteration and is followed by chalcopyrite. (2) The supergene enrichment zone is characterized by

chalcocite and digenite stockwork veins and veinlets. Chalcopyrite and pyrite are completely or partially replaced by chalcocite, digenite, and covellite. Supergene sulfides also occur interstitially to supergene pyrite grains. (3) The leached cap contains residual malachite, chalcantite, native copper and Fe oxides/ sulfate (e.g., jarosite, goethite, and hematite) produced by weathering of pyrite and chalcopyrite. The cap locally overlies the supergene sulfide enrichment zone and has a reddish color. Turquoise veins are surprisingly abundant in this zone and occur at shallow depths and along fractures extending deeper [34].

According to, detailed studies of the mineralogy/petrography, and, chemistry of a large number of drill cores and outcrop samples from various parts of the intrusive, four hypogene alteration zones are distinguished at the deposit, which include potassic, transition (sodic-potassic), phyllic, and Propylitic. Potassic alteration is the earliest alteration with potassic mineral assemblages and pervasive intense development formed as halos around deep veinlet systems. It consists of K-feldspar, crystals of Mg-enriched secondary biotite, and anhydrite. The propylitic alteration has a thickness about 400 m and main minerals are ubiquitous epidote, chlorite (\pm pyrite \pm calcite) and plagioclase. The transition alteration is located in the central part of cupola and large zone of sodic alteration is overprinted on potassic alteration. The phyllic alteration is typically low grade and contains chalcopyrite \pm pyrite \pm quartz veins except for intervals within ca. 100–250 m [34].

3. Borehole dataset

The borehole dataset plays an important role in geoscience investigations in both mineral exploration and grade estimation. A total of 153 boreholes were drilled in the study area in which, 49 of them belonged to the pre-drilled boreholes (MD series) with a total length of 26,961 m, 100 boreholes were related to MDK series boreholes with a total length of 33642 m and 4 boreholes associated with MDK-RC series boreholes with a total length 1300 m (**Figure 2**). The dataset included the collars, lithology, down-hole survey, and assay. The other acquired data for the study were zone, alteration, mineral and recovery. These samples with 2 m composites were analyzed by ICP-MS method for 44 elements at Zarazma laboratory, Tehran. Based on mineralogical, geological and geochemical results, it was found that the case study was favorable for the mineralization of Cu. The data was validated and subjected to statistical analysis. The histogram and descriptive statistics of the copper grades from 15952 samples in the hypogene zone of the case study are displayed in **Figure 3** and **Table 1**. The statistical parameters of Cu grade based on the lithology and alteration in the hypogene zone of the case study are also shown in **Table 2**. Accordingly, three lithology units consist of quartz-diorite, andesite and quartz-diorite dyke and three alteration zones composed of phyllic, potassic and propylitic accounted for more than 94% of the data length. The Cu regionalized variable was modeled by a second-order stationary random function. There was no trend of Cu concentration in any directions; this means that Cu concentration does not depend on the coordinates of the samples (**Figure 4 (a-c)**). Consequently, assumptions of the stationary are tenable.

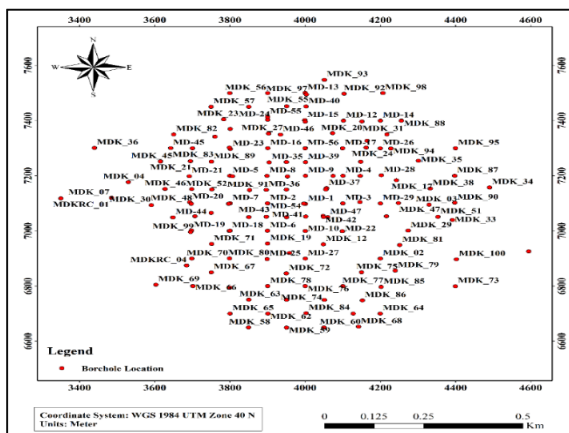


Figure 2. Borehole location map of the studied Cu porphyry deposit

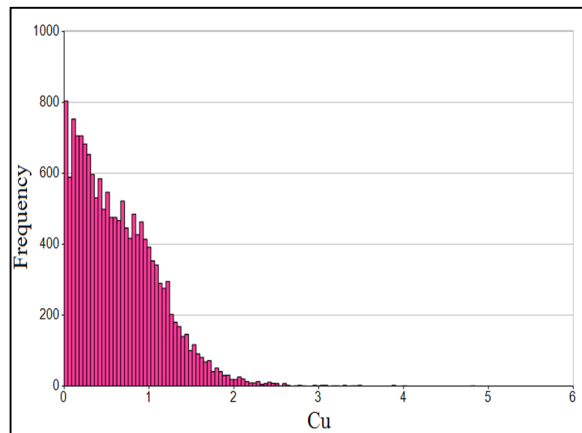


Figure 3. Histogram of the Cu raw data in the hypogene zone.

Table 1. Statistical parameters of the Cu element in the boreholes (raw data)

Variable	DL** (ppm)	Accuracy	Length* (m)	Mean	Min.	Max.	***StD	Variance	Skewness
Cu (%)	1	1	15952	0.643	0.001	4.8	0.480	0.231	1.011

* Some samples are removed from the study due to low value under the detection limit.

** Detection Limit

*** Standard Deviation

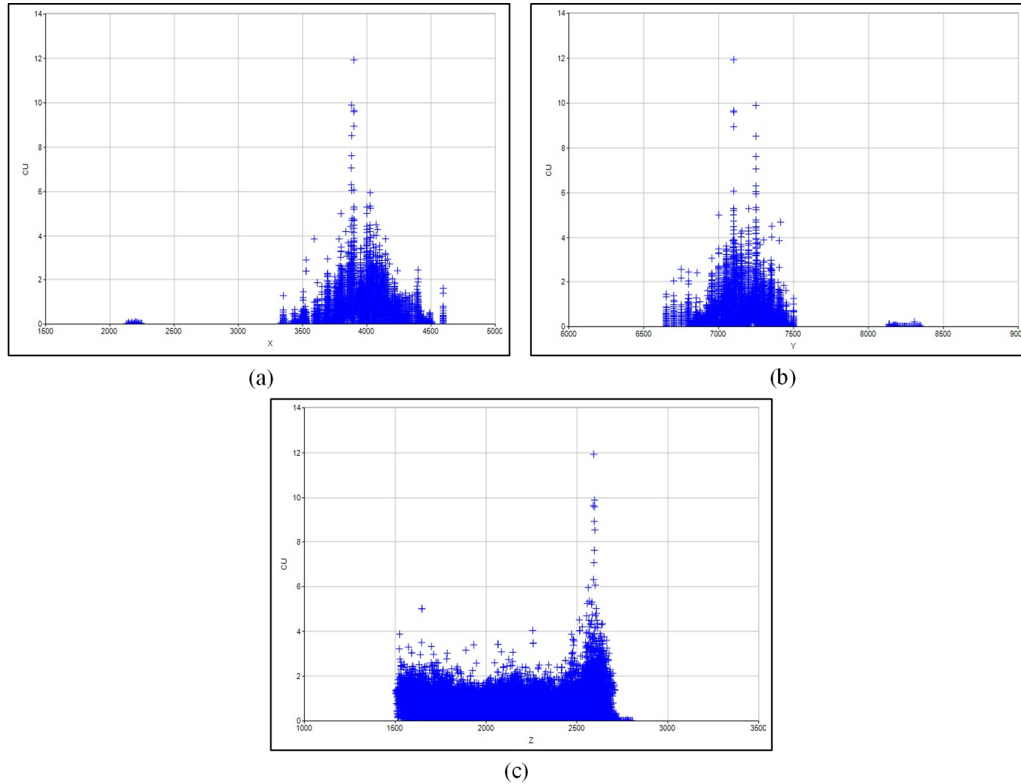


Figure 4. Variability of the Cu concentration in (a) east–west direction, (b) north–south direction and (c) depth within the hypogene zone

Table 2. Statistical parameters of the Cu grade based on the lithology and alteration in the hypogene zone.

		Length (m)	Length (%)	Cu (%)		
				Minimum	Maximum	Mean
Rock type	ANS	4968.35	15.32	0.0012	3	0.56
	ANS_QDI	166.5	0.513	0.02	1.45	0.83
	CLS	183.35	0.565	0.95	1.05	0.52
	DIA_D	14.2	0.043	0.01	0.06	0.02
	DIO_D	57.3	0.176	0.08	0.93	0.28
	GRD	861.4	2.65	0.28	2.75	1.039
	NBX	613.8	1.89	0.05	2.45	0.9
	QDI	23427	72.26	0.001	4.8	0.63
	QDI_ANS	88.3	0.27	0.07	1.6	0.88
	QDI_D	1260.9	3.88	0.0325	3.1	0.85
	QDI_GRD	72.75	0.224	0.09	1.44	0.53
TUF	584.75	1.80	0.002	2.16	0.12	
BLANK	120.3	0.37	0.02	1.36	0.60	
Alteration type	ARG	6	0.01	0.01	0.01	0.01
	CLS	12.3	0.03	-	-	-
	NA	590.05	1.82	0.02	1.08	2.45
	PHY	10930.5	33.71	0.001	0.31	4.04
	POT	19021.55	58.67	0	0.81	4.8
	PRP	137.6	0.42	0.01	0.13	0.6
	SER	23.75	0.07	0.12	0.56	1.62
	UNA	17	0.05	0.02	0.05	0.12
BLANK	1680.15	5.18	0.02	0.71	2.35	

4. Methods

In order to avoid increasing the volume of the article, the basics and principles of the methods used are not mentioned and the reader can refer to [35-40] to study the basics of OK method and [14, 26] for C-V fractal method. Here, only the WNN method is described

4.1. Wavelet Neural Networks (WNNs)

In the last decade, WNN has been considered as an alternative approach instead of ANN systems in many applications, since interpretation of the model with neural net is very difficult. The starting point of WNNs can be found in the work by Daugman [41] in which Gabor wavelets were used for image segmentation and then, Zhang and Benveniste (1992), Pati and Krishnaprasad (1993) have been developed these networks. Wavelet neural network systems typically approach grade variance and distribution as complex functions in space, approached by their various components. WNN combines the properties of the wavelet theory and the capabilities (i.e. pattern recognition, learning and memorization) of ANNs. They have attracted great interest in various fields of mathematics and engineering. The advantage of the WNN on the neural network is that training algorithms for WNN requires a smaller number of iterations compared to neural network and WNN use a wavelet as an activation function, instead of the classic sigmoidal family. In contrast to classical ANNs, WNs allow for constructive procedures that

efficiently initialize the parameters of the network [42-44].

4.1.1. Structure of a wavelet network

The WNN presented in this study for ore grade estimation has a three-layer structure. The lower layer represents the input layer, the middle layer is the hidden layer and the upper layer is the output layer. In the input layer the explanatory variables are introduced to the WN. The hidden layer consists of the hidden units (HUs) or wavelons. In this layer the input variables are transformed to dilated and translated version of the mother wavelet. Finally, in the output layer the approximation of the target values is estimated. The structure of the WNN is shown in **Figure 5**. The network output is given by the Equation (1):

$$y(t) = \sigma(x_n) = \sigma \left(\sum_{j=0}^M v_{ij} \psi_{a,b} \left(\sum_{k=0}^L w_{jk} x_k(t) \right) \right) \quad (i=1,2,\dots,N) \quad (1)$$

$$\sigma(x_n) = \frac{1}{(1 + e^{-x_n})}$$

ψ is the mother wavelet; y_i denotes the i th component of the output vector; x_k is the k th component of the input vector; v_{ij} is the connection weight between the output unit i and the hidden unit j ; w_{jk} denotes the weight between the hidden unit j and input unit k ; a_j and b_j are dilation and translation coefficient of wavelons in hidden layer respectively; L ; M ; N indicates the sum of input, hidden and output nodes respectively [42].

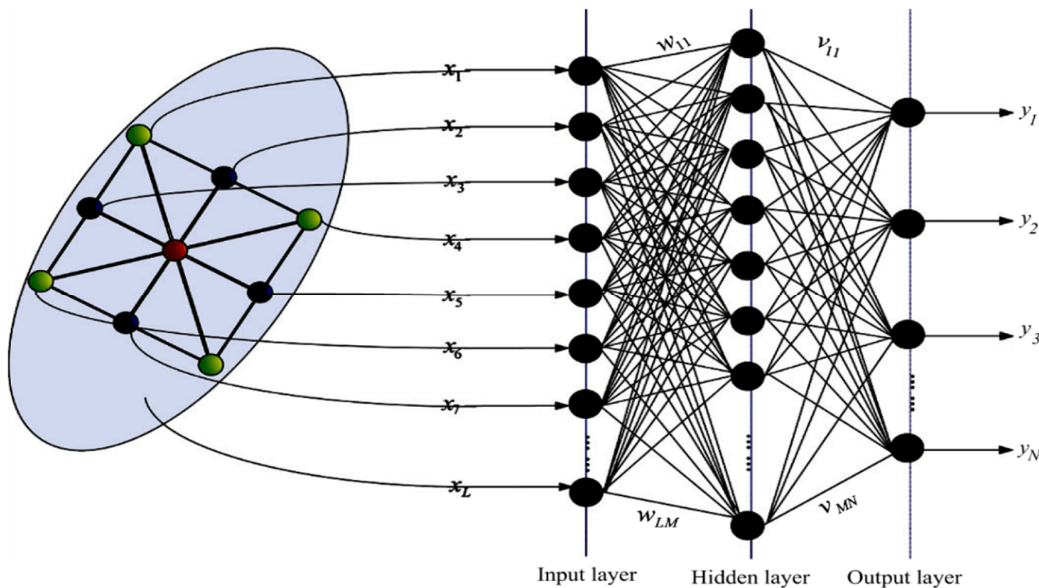


Figure 5. The structure of WNN network composed of one input layers, one hidden layer with wavelet activation function and one output layer [42]

4.1.2. Initialization of the parameters of the network

Choosing initial values of the network parameters is critical since random initialization affects the speed of training and may lead to a local minimum of the loss function. In other words, efficient initialization lead to less iterations in the training phase of the network and avoid of local minimums of the loss function in the training phase. In the past decades, different methods have been presented for efficient initialization of the wavelet parameters. In this study, Zhang and

Benveniste [45] methods has been employed for the initialization of translation and dilation parameters by Equations (2) - (3):

$$a_{jk} = 0.2(p_k - q_k) \tag{2}$$

$$b_{jk} = 0.5(p_k + q_k) \tag{3}$$

where p_k and q_k are defined as the maximum and minimum of input x_i . In the **Figure 6** the mother wavelets accompanied by their daughters are illustrated that are created using mentioned method [44, 70].

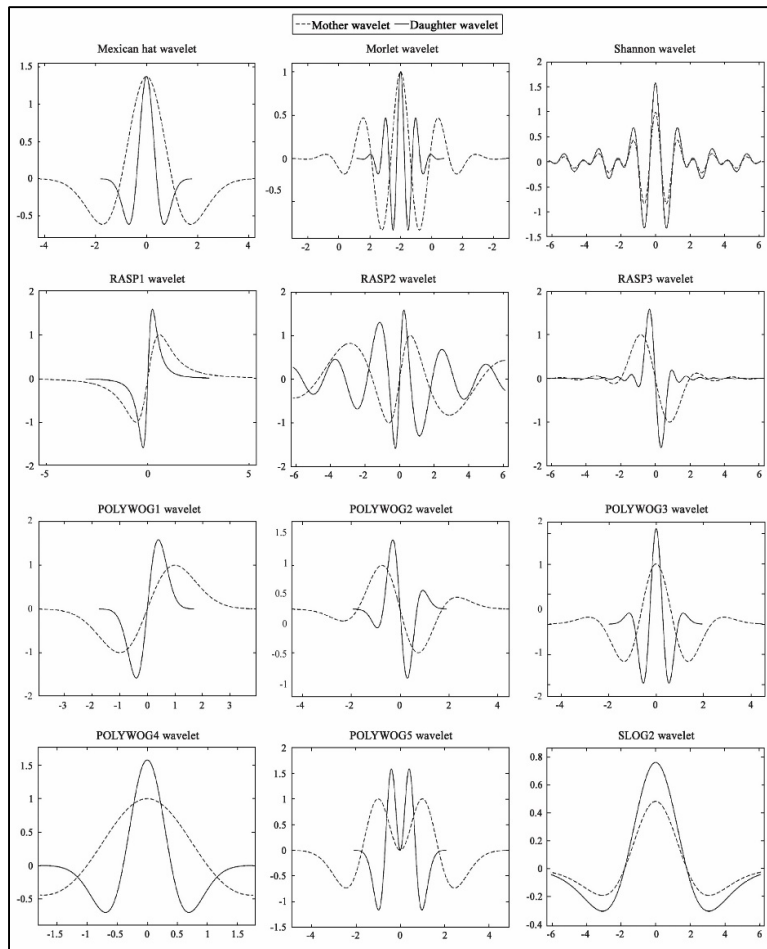


Figure 6. Different samples of mother wavelets with their daughters [42].

4.1.3. Training algorithm

After the initialization phase, the network is further trained in order to find the weights (w,v), translation (a), and dilation (b) which minimize the cost function. The main aim is to update the parameters during the training step. The cost function can be written as Equation (4) [42]:

$$E = \frac{1}{2} \sum_{p=1}^P \sum_{i=1}^N (d_i^p - y_i^p)^2 \tag{4}$$

whre the d_i^p is as the i th desired target output of p th input pattern. According to the above-mentioned reasoning based on the Scaled Conjugate Gradient (SCG) algorithm, and Levenberg–Marquardt (L-M) the training

algorithm is applied. The training algorithm diagram is shown in **Figure 7**.

4.1.4. Stopping Conditions for Training

Parameters of the WNN are training during the learning phase for approximation. The desired

function Scaled Conjugate Gradient and Levenberg–Marquardt methods have been applied for adjustable parameters. When variation of gradient and parameters reaches a lower bound or the number of iterations reaches a fixed maximum, training is stopped [42].

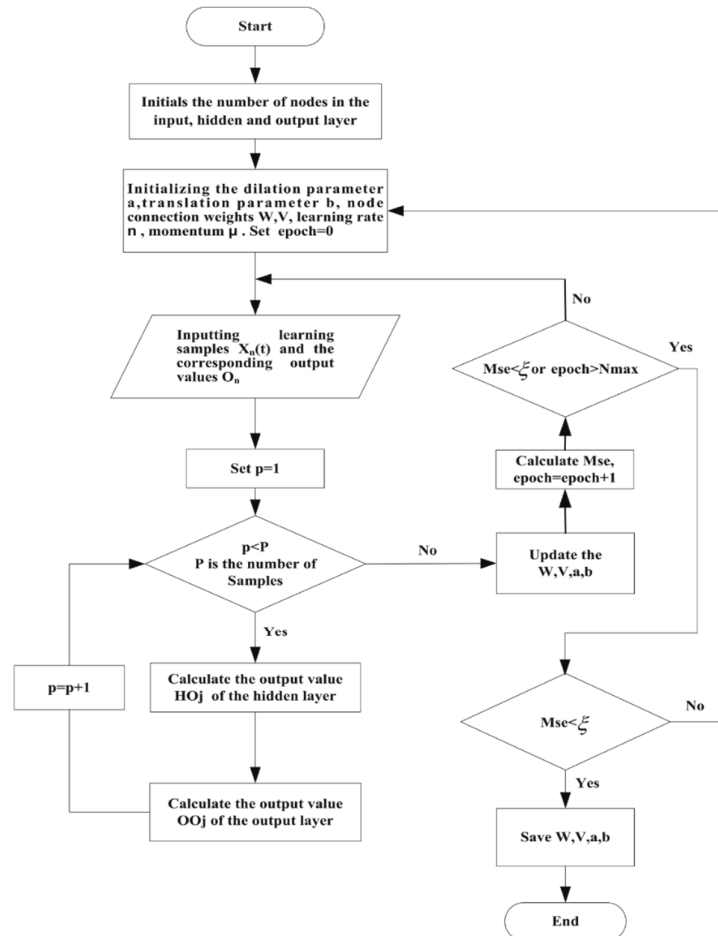


Figure 7. Learning algorithm for WNN.

5. Result and Discussion

5.1. Results of Ordinary Kriging (OK)

Here, the described data in Section 3 here is used to estimate the Cu grade. However, prior to the kriging calculations, it is necessary to carry out a series of data pre-processing. The first step is to determine and correct the outlier values. These values dramatically impact the statistical analysis and results interpretation.

High-grade values as outliers, are able to transform a mineral occurrence into an economic mineral deposit and may be sufficient to justify the development of a mining project [46, 47]. There are several ways to deal with the effects of the outlier values and control them. In this paper, the

box plot method is applied to remove outliers [48]. Another important issue in data preprocessing is the composite. In the other hand, it is very important to work with equal support (volume) samples [49]. In this study, the data for the analysis of Shahr-e-Babak resource by using the OK are divided into 2 m composites. According to the composite length, the lowest loss length is obtained while, the Cu grade and variance of Cu are similar to the original data.

Data variography for OK is the next step after the data preprocessing. Given the spatial variability and randomness, the variogram function can reflect the structure of spatial variability of a regionalized variable. The best way to describe spatial dependencies in the process of stationary is

covariance variogram. An omnidirectional semi-variogram of raw data along azimuth of 00°, Plunge of 00°, spread of 90°, and lag spacing of 60 m follows a spherical model with a nugget effect of 0.052 (%)² which reaches to a sill of 0.168 (%)² at a range of 410 m (Figure 8-a). To investigate anisotropy, directional semi-variograms were thereafter calculated and modelled with different directions with 30° horizontal angular increments, 15° horizontal angular tolerance, 30° vertical

angular increments and, 15° vertical angular tolerance in the hypogene zone of the porphyry ore deposit. The ore deposit has anisotropy because most of the variograms have different ranges. The main directions resulted from variography for 3 main directions of the search ellipsoid are presented in **Figure 8. (b)- (d)**. The directional semi-variogram model parameters are shown in **Table 3**.

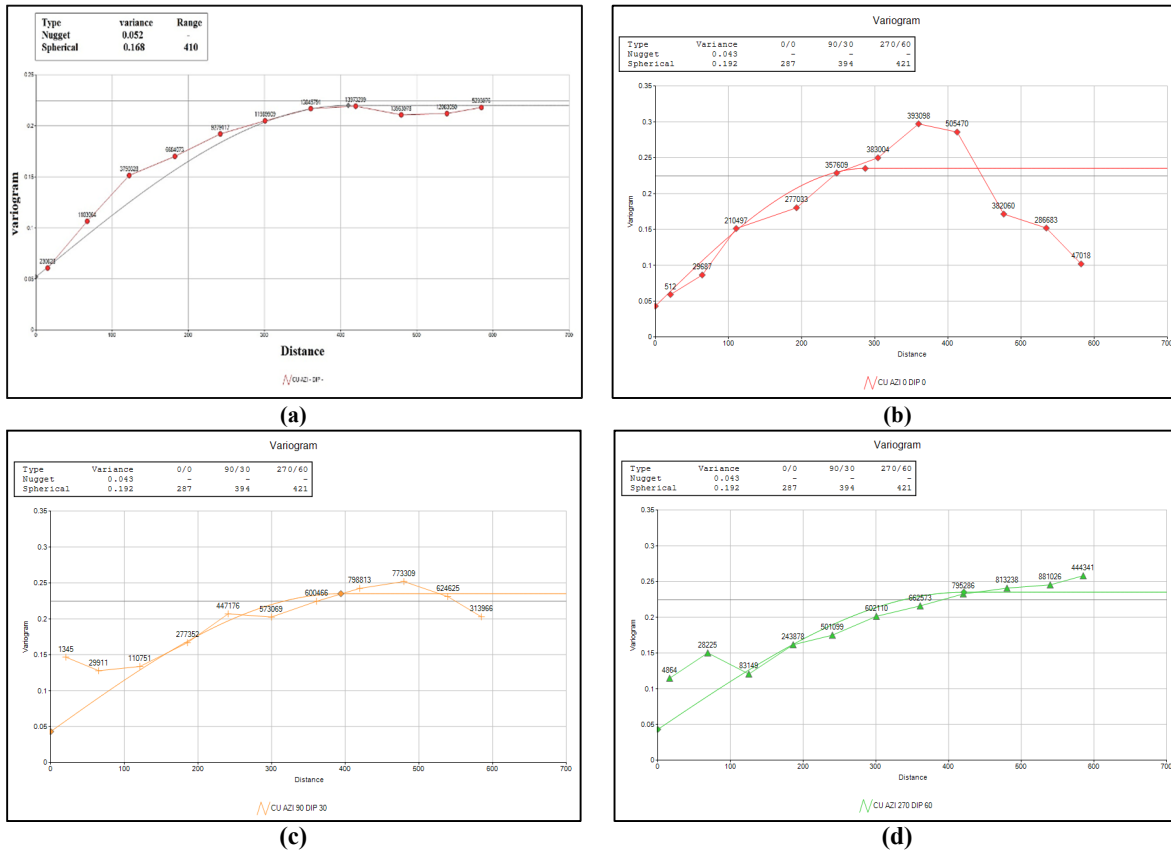


Figure 8. Experimental semi-variogram and appropriate fitted model of the (a) omnidirectional semi-variograms and (b) directional semi-variograms with Azimuth=0; Dip = 0 (c) directional semi-variograms with Azimuth=90; Dip = 30 (d) directional semi-variograms with Azimuth=270; Dip = 60 for 3 main directions of the search ellipsoid in the hypogene zone of porphyry ore deposit.

Table.3. directional Semi-variogram Parameters for 3 main directions of search ellipsoid in the hypogene zone of the porphyry ore deposit

Variogram model	Azimuth	Dip	nugget effect (%) ²	Range (m)	Threshold (%) ²
Spherical	0	0	0.043	287	0.192
Spherical	90	30	0.043	394	0.192
Spherical	270	60	0.043	421	0.192

The cross-validation method is used to validate the fitted model to the variogram of the hypogene zone. The correlation coefficient of the estimated values and actual values was partially acceptable and about 91%. Then, a block model was generated

from the ore body wireframe model using the block model tool in Data mine software. The parent cell size of 15 × 15 × 10 m corresponds to approximately one half the average drill hole spacing along strike, average mining width of the

deposit across strike and the likely mining bench height (10 m) in the vertical dimension respectively. Data search criteria employed took into account clustering of the local data, the geometry and continuity of local grade. The estimation and 3D modeling process are commenced from the elevation of 1300 m to 2700 m above the sea level in the mine. It also began from 3000 to 5010 m in the east direction and from 6500 to 7700 m in the north direction. The 3D

model of the Cu grade by OK in the Cu copper deposit is shown in **Figure 9**.

OK block models were validated to assess the accuracy of grade. Cross sectional views of color coded drill-hole composites were superimposed on similarly colour-coded block grades [17]. The best block model was the one whose colour codes compared closest to those of the sample grades. The obtained result are very suitable.

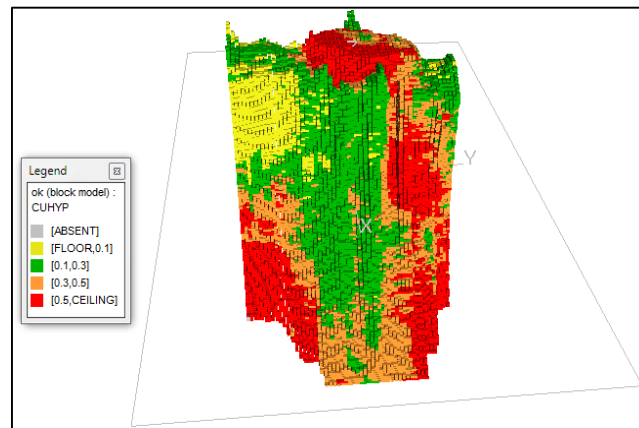


Figure 9. 3D model of the Cu concentration estimation by OK.

5.2. Results of wavelet Neural Networks (WNN)

In this study, a nonlinear WNN method is applied to estimate the Cu grade based on the borehole dataset. To obtain this aim, the below steps are followed:

5.2.1. Sample data acquisition

A sufficient amount of data is needed for ore grade estimation in train, validation, and test steps in WNN. In this paper, data on the porphyry copper deposit has been used. According to available reports, the deposit is non-homogeneous. The grades given are the actual grades of the boreholes. This dataset will be used to train and validation WNNs. The center points of cubes of dimension 15 m×15 m×10 m will be used to test.

5.2.2. Data preparation

The data pre-processing which is applied to train and validate the WNN topologies is discussed after the selection of the source data deposits. At the first stage of the modeling, the data is normalized which helps to scale the inputs and output and consequently leads to a better prediction. Scaling the inputs and output before applying ANN is very important. The main advantage is to avoid attributes in greater numeric ranges dominating

those in smaller numeric ranges. Another advantage is to avoid numerical difficulties during the calculation [20]. To normalize the data, different methods have been developed to improve the network training. In this study the input and output data are normalized by Equation (5).

$$X_{\text{norm}} = \frac{X - X_{\text{min}}}{X_{\text{max}} - X_{\text{min}}} \quad (5)$$

where x is the data which should be normalized, and x_{max} and x_{min} are the maximum and minimum of the original data, respectively. Moreover, X_{norm} is the transformed normalized data [50-52].

Divisionism as one of the most important issues would lead to inaccurate and illogical results if has not been considered properly. WNN's data are divided into three groups: 1) Training data: the obvious characteristic of this group is that they are definite and clear and are used during training process. 2) Test data: the characteristic of these data is that their target is not clear and they are used after training process. 3) Validation data: they are used to avoid over fitting, are not definite and are also used during training process. In this paper, all of the available datasets were divided randomly into three distinct subsets consisting of the training (70%), validation (15%) and testing (15%).

5.2.3. Performance of WNN

There are different error metrics to evaluate the accuracy of models, including coefficient of determination (R^2), EI, RMSE, mean bias error (MBE). In addition to these indices, persistence index (PI) and extrapolation index (EXI) are also included [53]. All selected indices (except the mean bias error and coefficient of extrapolation) also can be found in Crochemore et al. [54], which summarizes various error metrics for evaluating modeled hydrograph. The coefficient of determination (R^2), RMSE and Mean Absolute Error (MAE) were used in this study. R^2 measures the degree of correlation between the observed and the predicted values. A model's strength is measured by R^2 through developing a relationship between the input and output variables. The values of R^2 range from 0 to 1, in which 1 indicates a perfect fit between the data and the line drawn through them, and 0 represents no statistical correlation between the data and the line. R^2 is calculated by Equation (6) [55]:

$$R^2 = 1 - \frac{\sum_{k=1}^N (t_k - y_k)^2}{\sum_{k=1}^N (t_k - \bar{t}_k)^2} \quad (6)$$

where t_k and y_k are target and network outputs for the k th output, respectively; \bar{t}_k is the average of the targets and N is the total number of the considered events.

The root mean square error (RMSE) indicates the discrepancy between the observed and the calculated values. The lower the RMSE, the more accurate is the prediction and is given by Equation (7) [55]:

$$RMSE = \sqrt{\frac{\sum_{i=1}^N (y_i - \bar{y}_i)^2}{N}} \quad (7)$$

where y_i is the observed data, \bar{y}_i is the calculated data and, N is the number of the observations. A perfect fit between observed and forecasted values has an RMSE of 0. The best fit between observed and calculated values, which is unlikely to occur, would have R^2 as 1 and RMSE as 0.

Mean Absolute Error (MAE) is as Eq. (8):

$$MAE = \frac{1}{N} \sum_{i=1}^N |y_i - \bar{y}_i| \quad (8)$$

5.2.4. Modeling of WNN

All the mentioned properties such as data selection, pre-processing and WNN's parameters, were selected and considered for the modeling. In contrast, standard feed forward neural networks which in the activation function of hidden layer neurons is a sigmoid function in order to increase their performance generality, activation functions are substituted with different daughter wavelet functions to create various WNNs. Different wavelet function formulas are shown as activation functions in **Table. 4**. **Table.5** summarized the results obtained from data the neural network adaptive wavelet (WNN) model.

The numbers of hidden layers and neurons were selected by a number of repeated trials and estimated errors in this study. According to **Table. 5** the optimal results were obtained when one hidden layer with 5 neurons with Morlet activation function was used for training which have the smallest RMSE and greater R^2 compared compared to other activation networks. The number of inputted neurons corresponds to the three inputted i.e. x coordinate, y coordinate and z coordinate. The output layer has one neurons corresponding to the Cu grades. The WNN, when combined with the architecture and the saved weights, and evaluate with validation data can be used to predict the test points. **Figure10** show the 3D model of the Cu grade by WNN in the Cu copper deposit.

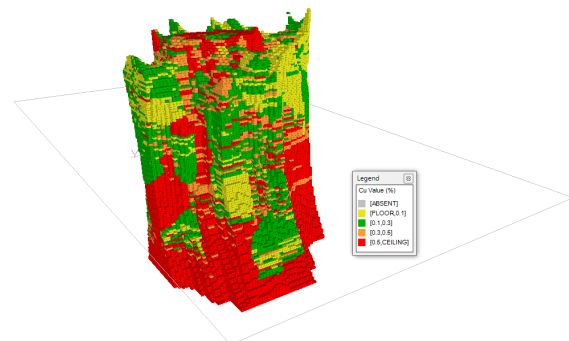


Figure 10. 3D model of the Cu concentration estimation by WNN.

Table.4. Proposed wavelets for the application in WNN

Case number	Name	$h(\tau)$	$\frac{\partial h(\tau)}{\partial b}$
1	Morlet	$\cos(\omega_0 \tau) \exp(-0.5 \tau^2)$	$\frac{1}{a} [\omega_0 \sin(\omega_0 \tau) \exp(-0.5 \tau^2) + \tau h(\tau)]$
2	Mexican hat	$(\tau^2 - 1) \exp(-\frac{\tau^2}{2})$	$(3\tau - \tau^3) \exp(-\frac{\tau^2}{2})$
3	RASP1	$\frac{\tau}{(\tau^2 + 1)^2}$	$\frac{1}{a} \frac{(3\tau^2 - 1)}{(\tau^2 + 1)^3}$
4	RASP2	$\frac{\tau \cos \tau}{\tau^2 + 1}$	$\frac{\tau (\frac{\tau^2 + 1}{a}) \sin(\tau) + (\frac{\tau^2 - 1}{a}) \cos(\tau)}{(\tau^2 + 1)^2}$
5	RASP3	$\frac{\sin(\pi \tau)}{\tau^2 - 1}$	$\frac{(\frac{2\tau}{a}) \sin(\pi \tau) - \pi (\frac{\tau^2 - 1}{a}) \cos(\pi \tau)}{(\tau^2 - 1)^2}$
6	SLOG1	$\frac{1}{1 + e^{-\tau+2}} - \frac{1}{1 + e^{-\tau+3}} - \frac{1}{1 + e^{-\tau-3}} + \frac{1}{1 + e^{-\tau-1}}$	$\frac{1}{a} [-\frac{e^{-\tau+1}}{(1 + e^{-\tau+1})^2} - \frac{e^{-\tau+3}}{(1 + e^{-\tau+3})^2} - \frac{e^{-\tau-3}}{(1 + e^{-\tau-3})^2} + \frac{e^{-\tau-1}}{(1 + e^{-\tau-1})^2}]$
7	SLOG2	$\frac{3}{1 + e^{-\tau-1}} - \frac{3}{1 + e^{-\tau+1}} - \frac{1}{1 + e^{-\tau-3}} + \frac{1}{1 + e^{-\tau+3}}$	$\frac{1}{a} [-\frac{3e^{-\tau-1}}{(1 + e^{-\tau-1})^2} - \frac{3e^{-\tau+1}}{(1 + e^{-\tau+1})^2} - \frac{e^{-\tau-3}}{(1 + e^{-\tau-3})^2} + \frac{e^{-\tau+3}}{(1 + e^{-\tau+3})^2}]$
8	POLYWOG1	$\tau \exp(-\frac{\tau^2}{2})$	$\frac{1}{a} (\tau^2 - 1) \exp(-\frac{\tau^2}{2})$
9	POLYWOG2	$(\tau^3 - 3\tau) \exp(-\frac{\tau^2}{2})$	$\frac{1}{a} (\tau^4 - 6\tau^2 + 3) \exp(-\frac{\tau^2}{2})$
10	POLYWOG3	$(\tau^4 - 6\tau^2 + 3) \exp(-\frac{\tau^2}{2})$	$\frac{1}{a} (\tau^5 - 10\tau^3 + 15\tau) \exp(-\frac{\tau^2}{2})$
11	POLYWOG4	$(1 - \tau^2) \exp(-\frac{\tau^2}{2})$	$\frac{1}{a} (3\tau - \tau^3) \exp(-\frac{\tau^2}{2})$
12	POLYWOG5	$(3\tau^2 - \tau^4) \exp(-\frac{\tau^2}{2})$	$\frac{1}{a} (-\tau^5 + 7\tau^3 - 6\tau) \exp(-\frac{\tau^2}{2})$
13	Shannon	$\frac{\sin 2\pi\tau - \sin \pi\tau}{\pi\tau}$	$\frac{\pi}{a} \frac{(-\pi\tau \cos \pi\tau - 2\pi \cos \pi\tau + \sin \pi\tau - \sin 2\pi\tau)}{(\pi\tau)^2}$

Table.5. Results of the observed and predicted data obtained from the WNN. The best obtained network is in bold.

Number	Wavelet name	Number of Neurons	RMSE			MAE			Determination Coefficient (R ²)		
			Train	test	validation	Train	test	validation	Train	test	validation
1	Shannon	6	6.21	7.481	7.25	5.20	5.73	5.46	0.71	0.86	0.83
2	Mexican hat	7	4.08	6.21	5.73	2.29	5.83	5.39	0.95	0.82	0.87
3	Morlet	5	3.31	3.75	3.22	1.53	3.10	2.14	0.84	0.96	0.92
4	POLYWOG1	8	8.34	5.76	6.43	5.98	4.98	4.25	0.62	0.64	0.67
5	POLYWOG2	5	7.29	4.26	5.68	3.53	3.22	3.67	0.76	0.81	0.88
6	POLYWOG3	7	7.97	6.46	6.21	5.98	5.23	5.44	0.63	0.56	0.53
7	POLYWOG4	8	2.24	6.54	5.14	8.15	4.9	3.16	0.75	0.55	0.61
8	POLYYOG5	6	5.49	6.18	6.23	3.72	5.03	5.95	0.83	0.60	0.79
9	SLOG1	4	5.96	5.56	5.86	3.45	5.11	4.98	0.79	0.68	0.78
10	SLOG2	9	6.57	5.73	5.31	4.18	4.83	4.75	0.72	0.68	0.72
11	RASP1	8	7.72	6.98	6.32	5.46	5.17	5.42	0.66	0.58	0.58
12	RASP2	9	5.89	5.67	5.43	3.98	4.47	4.13	0.75	0.67	0.77
13	RASP3	6	7.67	5.98	5.39	4.44	5.68	5.32	0.67	0.74	0.81

A comparison between two methods of WNN and OK showed that, both methods are able to estimate cu grade very well. Nevertheless, the WNN is faster and non-linear estimator. The advantage of the WNN method is that it does not

require any pre-processing or need to carry out variogram operations. It also can be used for initial data without any special pre-processing however, OK algorithms smooth the data, and thus, their application in pre-processing of data for fractal

analysis is not suitable. In the next subsection, the results of the WNN are been used in the determination of alteration zones in the Shahr-e-Babak porphyry copper deposit.

5.3. Results of Concentration-Area (C-V) fractal model

The C-V fractal model can be considered as a proper method to describe spatial distributions of different attributes (ore elements in this scenario) within the various ore bodies. Using the 3D model

of Cu distribution obtained from OK and WNN in the porphyry ore deposit, the C-V log-log plot was calculated (Figure 11). The data pairs of the concentrations and volumes were projected to log-log graphs and linear regression was applied to fit straight lines. The coefficient of determination R^2 ($0 \leq R^2 \leq 1$) was calculated to evaluate the effect of linear regression. The regression line was determined via adjusting it to achieve the largest coefficient of determination. Consequently, two threshold values and three populations were obtained (Table. 6).

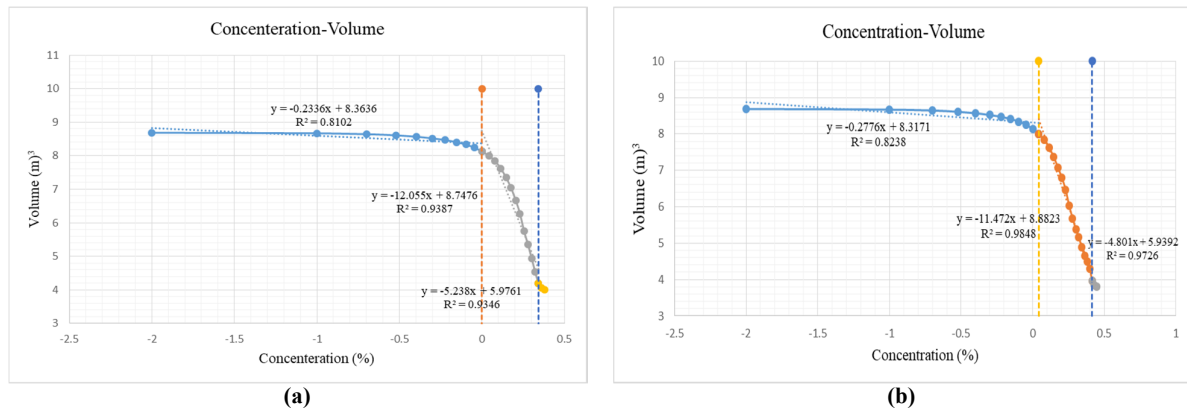


Figure 11. C-V fractal log-log plots resulted from the (a) OK and (b) WNN modeling.

Table. 6. Cu (%) threshold value obtained from the C-V plot

population	Cu (%) threshold value (OK)	Cu (%) threshold value (WNN)
Population 1	$0 \leq \text{Cu} (\%) < 1$	$0 \leq \text{Cu}(\%) < 1.1$
Population 2	$1 \leq \text{Cu} (\%) < 2.2$	$1.1 \leq \text{Cu}(\%) < 2.5$
Population 3	$2.2 \leq \text{Cu} (\%) < 2.4$	$2.5 \leq \text{Cu} (\%) < 2.8$

5.4. Comparison between fractal and spatial alteration models

In order to validate the results obtained through the C-V fractal modeling, the models are compared to the 3D alteration zone models of the Shahr-e-Babak porphyry copper deposit' zone comprising the phyllic and potassic zones (Figure 12). The models are generated by applying the Datamine studios software and the geological drill core data.

To calculate spatial correlations between two binary models, especially mathematical and geological ones, logratio matrix can be applied. The comparison between C-V fractal model results and geological model of the alteration zones is carried out to obtain the number of overlapped voxels (A, B, C and D). Using the obtained numbers, Type I error (T1E), Type II error (T2E), and overall accuracy (OA) of different fractal populations are estimated for each one of the alteration zones.

Alteration models have a key role in zone delineation and also in presenting geological models. Potassic alteration in Lowell and Guilbert [1] model hosts of high grade Cu mineralization and located in the central part of Cu porphyry deposits. Based on these models, phyllic alterations host major mineralization in supergene enrichment and hypogene zones. The first cu threshold is 1% in Ok estimation and 1.1% in WNN estimation, and values of <1% or 1.1% Cu refer to phyllic alteration. The second Cu threshold is 2.2% in Ok and 2.5 % in WNN, and values of >2.2 or 2.5 % Cu indicate potassic alteration. Results of C-V modeling of the porphyry ore deposit are compared to the 3D geological model of the deposit constructed by utilizing the Data mine v.3.24 software. There is good correlation between both the geological and C-V fractal models for phyllic and potassic alterations. This was quantitatively proved by a matrix of number of overlapping voxels in the geological and C- v fractal models

(Figure 12, Table. 7 and Table.8). The result of matrix was shown that C-V Fractal model resulted from WNN has better correspondence with geological model.

There is spatial coincidence between alteration zones defined by the C–V and WNN modeling and the zones defined by modeling of geological drill

core data. The propylitic alteration derived via C–V and WNN modeling occurs in marginal parts of the area which has good correlation with geological data in the case study. However, potassic alteration obtained by WNN and C–V modeling is situated in the central part of a study area which confirmed the geological data (Figure 12).

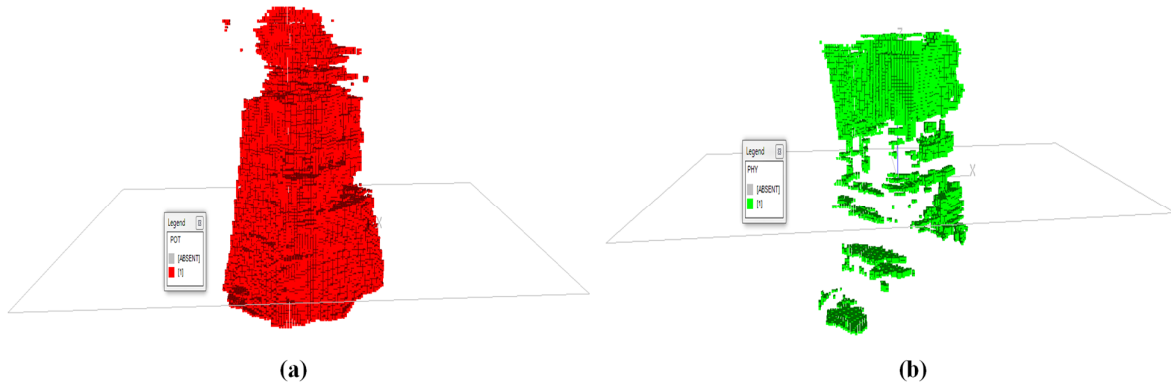


Figure 12. Alteration zones in hypogene zone based of geological model: (a) potassic, and (b) phyllic alteration

Table 7. OA, T1E and T2E resulted from Comparison between the Phyllic alteration zone in 3D geological model and threshold values of Cu in C–V fractal model resulted from Ok and WNN in hypogene zone.

		Geological model			
		Inside zone		outside zone	
Fractal model	Inside zone	True positive (A)		False positive (B)	
	Outside zone	False negative (C)		True negative (D)	
		Type I Error = C / (A + C)		Type II Error = B / (B + D)	
		Overall accuracy = (A + D) / (A + B + C + D)			
		Phyllic alteration of geological model			
		Inside zones		Outside zones	
C–V fractal model of Neural network (0 < Cu < 1)	Inside zones	A	86630	B	103504
	Outside zones	C	2758	D	159362
		T1E	0.03	T2E	0.39
		OA	0.68		
C–V fractal model of Neural network (1 ≤ Cu < 2.2)	Inside zones	A	864	B	32986
	Outside zones	C	18860	D	139085
		T1E	0.95	T2E	0.19
		OA	0.72		
C–V fractal model of Neural network (Cu ≥ 2.2)	Inside zones	A	0	B	9
	Outside zones	C	33290	D	216349
		T1E	1	T2E	0.00004
		OA	0.86		
C–V fractal model of Ordinary Kriging (0 < Cu < 1.1)	Inside zones	A	75557	B	101203
	Outside zones	C	3758	D	139342
		T1E	0.04	T2E	0.42
		OA	0.67		
C–V fractal model of Ordinary Kriging (1.1 ≤ Cu < 2.5)	Inside zones	A	654	B	39986
	Outside zones	C	26860	D	139085
		T1E	0.97	T2E	0.22
		OA	0.67		
C–V fractal model of Ordinary Kriging (Cu ≥ 2.5)	Inside zones	A	0	B	7
	Outside zones	C	33289	D	183062
		T1E	1	T2E	3.0.00001
		OA	0.84		

Table 8. OA, T1E and T2E resulted from Comparison between the potassic alteration zone in 3D geological model and threshold values of Cu in C–V fractal model resulted from Ok and WNN in hypogene zone.

		Potassic alteration of geological model			
		Inside zones		Outside zones	
C–V fractal model of Neural network (0<Cu<1)	Inside zones	A	21763	B	7523
	Outside zones	C	81230	D	242282
		T1E	0.78	T2E	0.03
		OA	0.74		
C–V fractal model of Neural network (1≤Cu<2.2)	Inside zones	A	11647	B	2724
	Outside zones	C	91231	D	228186
		T1E	0.88	T2E	0.01
		OA	0.72		
C–V fractal model of Neural network (Cu ≥2.2)	Inside zones	A	17	B	8
	Outside zones	C	101698	D	240789
		T1E	0.99	T2E	0.0003
		OA	0.7		
C–V fractal model of Ordinary Kriging (0<Cu<1.1)	Inside zones	A	12999	B	2433
	Outside zones	C	95876	D	218492
		T1E	0.88	T2E	0.01
		OA	0.70		
C–V fractal model of Ordinary Kriging (1.1≤Cu<2.5)	Inside zones	A	4245	B	1517
	Outside zones	C	106421	D	229415
		T1E	0.96	T2E	0.006
		OA	0.68		
C–V fractal model of Ordinary Kriging (Cu≥2.5)	Inside zones	A	6	B	2
	Outside zones	C	102871	D	240822
		T1E	0.99	T2E	0.00001
		OA	0.68		

6. Conclusions

Modeling of alteration zones is one of the most important stage in mineral exploration Project. Alteration modeling is complicated and should be consistent with geological interpretation. Conventional modeling based on drill core logging is often descriptive along with uncertainty and lack of proper recognition of alteration zones. This type of modeling does not consider ore grades whereas ore grade is very important variable and there is an obvious correlation between alteration patterns and grade distribution. In the Other hands, spatial structure of alteration zones can be determined via ore grades. In this paper, a combination of Wavelet Neural Network (WNN) and Concentration–Volume (C–V) fractal methods was used to delineate the alteration regions in the hypogene zone of porphyry ore deposit, Shahr-e-Babak district, SE Iran. At first, the applicability of wavelet neural network (WNN) technique for ore grade estimation was examined which is based on integration between wavelet theory and Artificial Neural Network (ANN). The outcome is compared with Ordinary Kriging (OK). Then, estimates

obtained from WNN and OK to delineate the potassic and phyllic alteration regions in the hypogene zone of Cu porphyry deposit was used in Concentration–Volume (C–V) fractal model. According to correlation derived from log ratio matrix, which was used to compare between geological model and quantitative modeling obtained from C–V fractal model and WNN, was shown that Cu values less than 1.1% from WNN has more overlapped voxels with phyllic alteration zone by overall accuracy (OA) of 0.74. Spatial correlation between the potassic alteration zones resulted from 3D geological modeling and high concentration zones in C–V fractal model shows that the alteration zone has Cu values between 1.1% and 2.2% with OA of 0.72 and finally have an appropriate overlap with Cu values greater than 2.2% with OA of 0.7. Generally, the results showed that the wavelet network (WNN, Morlet) with OA greater than OK would be an appropriate substitute for determining alteration zones.

References

- [1]. Lowell, J.D. and Guilbert, J.M. (1970). Lateral and vertical alteration-mineralization zoning in porphyry ore deposits. *Economic Geology* 65, 373-408.
- [2]. Hezarkhani, A. and Williams-Jones, A.E. (1998). Controls of alteration and mineralization in the Sungun porphyry copper deposit, Iran; evidence from fluid inclusions and stable isotopes. *Economic Geology* 93, 651-670.
- [3]. Asghari, O., Hezarkhani, A. and Soltani, F. (2009). The comparison of alteration zones in the Sungun porphyry copper deposit, Iran (based on fluid inclusion studies). *Acta Geologica Polonica* 59, 93-109.
- [4]. Soltani, F., Afzal, P. and Asghari, O. (2014). Delineation of alteration zones based on Sequential Gaussian Simulation and concentration-volume fractal modeling in the hypogene zone of Sungun copper deposit, NW Iran. *Journal of Geochemical Exploration* 140, 64-76.
- [5]. Schwartz, G.M. (1947). Hydrothermal alteration in the "porphyry copper" deposits. *Economic Geology* 42, 319-352.
- [6]. Beane, R. (1982). Hydrothermal alteration in silicate rocks. University of Arizona Press, Tucson, pp. 117-137.
- [7]. Roedder, E. (1971). Fluid inclusion studies on the porphyry-type ore deposits at Bingham, Utah, Butte, Montana, and Climax, Colorado. *Economic Geology* 66, 98-118.
- [8]. Nash, J.T. (1976). Fluid-inclusion petrology data from porphyry copper deposits and applications to exploration: a summary of new and published descriptions of fluid inclusions from 36 porphyry copper deposits and discussion of possible applications to exploration for copper deposits. US Govt. Print. Off.
- [9]. Sillitoe, R. 1997. Characteristics and controls of the largest porphyry copper-gold and epithermal gold deposits in the circum-Pacific region. *Australian Journal of Earth Sciences* 44, 373-388.
- [10]. Ulrich, T., Günther, D. and Heinrich, C.A. (2002). The evolution of a porphyry Cu-Au deposit, based on LA-ICP-MS analysis of fluid inclusions: Bajo de la Alumbrera, Argentina. *Economic Geology* 97, 1889-1920.
- [11]. Asghari, O. and Hezarkhani, A. (2008). Applying discriminant analysis to separate the alteration zones within the Sungun porphyry copper deposit. *Journal of Applied Sciences* 24, 4472-4486.
- [12]. Berger, B.R., Ayuso, R.A., Wynn, J.C. and Seal, R.R. (2008). Preliminary model of porphyry copper deposits. US geological survey open-file report 1321, 55.
- [13]. Afzal, P., Alghalandis, Y.F., Moarefvand, P., Omran, N.R. and Haroni, H.A. (2012). Application of power-spectrum-volume fractal method for detecting hypogene, supergene enrichment, leached and barren zones in Kahang Cu porphyry deposit, Central Iran. *Journal of Geochemical Exploration* 112, 131-138.
- [14]. Afzal, P., Madani, N., Shahbeik, S. and Yasrebi, A.B. (2015). Multi-Gaussian kriging: a practice to enhance delineation of mineralized zones by Concentration-Volume fractal model in Dardevey iron ore deposit, SE Iran. *Journal of Geochemical Exploration* 158, 10-21.
- [15]. Emery, X. (2008). Uncertainty modeling and spatial prediction by multi-Gaussian kriging: accounting for an unknown mean value. *Computers & Geosciences* 34, 1431-1442.
- [16]. Chiles, J.-P. and Delfiner, P. (2009). *Geostatistics: modeling spatial uncertainty*. John Wiley & Sons.
- [17]. Rossi, M.E. and Deutsch, C.V. 2013. *Mineral resource estimation*. Springer Science & Business Media.
- [18]. Cheng, Q., Xu, Y. and Grunsky, E. (2000). Integrated spatial and spectrum method for geochemical anomaly separation. *Natural Resources Research* 9, 43-52.
- [19]. Zuo, R., Cheng, Q., Agterberg, F.P. and Xia, Q. (2009). Evaluation of the uncertainty in estimation of metal resources of skarn tin in Southern China. *Ore Geology Reviews* 35, 415-422.
- [20]. Li, X.-l., Li, L.-h., Zhang, B.-l. and Guo, Q.-j. (2013). Hybrid self-adaptive learning based particle swarm optimization and support vector regression model for grade estimation. *Neurocomputing* 118: 179-190.
- [21]. Wang, H. and Zuo, R. (2015). A comparative study of trend surface analysis and spectrum-area multifractal model to identify geochemical anomalies. *Journal of Geochemical Exploration* 155: 84-90.
- [22]. Soltani, F., Moarefvand, P., Alinia, F. and Afzal, F. (2020). Detection of main rock type for Rare Earth Elements (REEs) mineralization using staged factor and fractal analysis in Gazestan iron-apatite deposit, central iran. *Geopersia* 10 (1): 89-99.
- [23]. Mirzaie, M., Afzal, P. Adib, A., Rahimi, E. and Mohammadi, G. (2020). Detection of zones based on ore and gangue using fractal and multivariate analysis in Chah Gaz iron ore deposit, central iran. *Journal of Mining and Environment* 11 (2): 453-466.
- [24]. Yasrebi, A.B. and Hezarkhani, A. (2019). Resources classification using fractal modelling in eastern Kahang Cu-Mo porphyry deposit, central iran. *Iranian Journal of Earth Sciences* 11 (1): 56-67.
- [25]. Daneshvar Saein, L. (2017). Delineation of enriched zones of Mo, Cu and Re by concentration-

volume fractal model in Nowchun Mo-Cu porphyry deposit, SE Iran. *Iranian Journal of Earth Sciences* 9 (1): 64-72.

[26]. Afzal, P. and Zahedi, P. (2018). determination of phosphorous and sulfur zonation using fractal modeling in jalalabad iron ore, se iran. *International Multidisciplinary Scientific GeoConference: SGEM* 18 (1.3). 247-254.

[27]. Dutta, S., Misra, D., Ganguli, R., Samanta, B. and Bandopadhyay, S. (2006). A hybrid ensemble model of kriging and neural network for ore grade estimation. *International Journal of Surface Mining, Reclamation and Environment* 20. 33-45.

[28]. Samanta, B. and Bandopadhyay, S. (2009). Construction of a radial basis function network using an evolutionary algorithm for grade estimation in a placer gold deposit. *Computers & Geosciences* 35. 1592-1602.

[29]. Samanta, B. (2010). Radial basis function network for ore grade estimation. *Natural resources research* 19. 91-102.

[30]. Tahmasebi, P., Hezarkhani, A. (2012). A hybrid neural networks-fuzzy logic-genetic algorithm for grade estimation. *Computers & geosciences* 42. 18-27.

[31]. Reis, A., Sousa, A. and Fonseca, E.C. (2003). Application of geostatistical methods in gold geochemical anomalies identification (Montemor-O-Novo, Portugal). *Journal of Geochemical Exploration* 77. 45-63.

[32]. Subbey, S., Christie, M. and Sambridge, M. (2004). Prediction under uncertainty in reservoir modeling. *Journal of Petroleum Science and Engineering* 44. 143-153.

[33]. Berberian, M. and King, G. (1981). Towards a paleogeography and tectonic evolution of Iran. *Canadian journal of earth sciences* 18. 210-265.

[34]. Hezarkhani, A. (2008). Hydrothermal evolution of the Miduk porphyry copper system, Kerman, Iran: a fluid inclusion investigation. *International Geology Review* 50. 665-684.

[35]. Dai, F., Zhou, Q., Lv, Z., Wang, X. and Liu, G. (2014). Spatial prediction of soil organic matter content integrating artificial neural network and ordinary kriging in Tibetan Plateau. *Ecological Indicators* 45. 184-194.

[36]. Isaaks, E., Srivastava, R. (1989). *Applied geostatistics: An introduction*. Applied geostatistics: An introduction to.

[37]. Matheron, G. (1962). *Traité de géostatistique appliquée*. 1 (1962). Editions Technip.

[38]. Pokhrel, R.M., Kuwano, J. and Tachibana, S. (2013). A kriging method of interpolation used to map liquefaction potential over alluvial ground. *Engineering geology* 152. 26-37.

[39]. Vann, J. and Guibal, D. (1998). Beyond Ordinary Kriging—An overview of non-linear estimation, *Proceedings of a one day symposium: Beyond Ordinary Kriging*.

[40]. Hu, H. and Shu, H. (2015). An improved coarse-grained parallel algorithm for computational acceleration of ordinary Kriging interpolation. *Computers & Geosciences* 78. 44-52.

[41]. Daugman, J.G. (1988). Complete discrete 2-D Gabor transforms by neural networks for image analysis and compression. *IEEE Transactions on Acoustics, Speech, and Signal Processing* 36. 1169-1179.

[42]. Alexandridis, A.K. and Zaprakis, A.D. (2013). Wavelet neural networks: A practical guide. *Neural Networks* 42. 1-27.

[43]. Saljooghi, B.S. and Hezarkhani, A. (2014). Comparison of WAVENET and ANN for predicting the porosity obtained from well log data. *Journal of Petroleum Science and Engineering* 123. 172-182.

[44]. Saljooghi, B.S. and Hezarkhani, A. (2015). A new approach to improve permeability prediction of petroleum reservoirs using neural network adaptive wavelet (wavenet). *Journal of Petroleum Science and Engineering* 133. 851-861.

[45]. Zhang, Q. and Benveniste, A. (1992). Wavelet networks. *IEEE transactions on Neural Networks* 3. 889-898.

[46]. Cousineau, D. and Chartier, S. (2010). Outliers detection and treatment: a review. *International Journal of Psychological Research* 3.

[47]. Costa, J.F. (2003). Reducing the impact of outliers in ore reserves estimation. *Mathematical geology* 35. 323-345.

[48]. Schwertman, N.C., Owens, M.A. and Adnan, R. (2004). A simple more general boxplot method for identifying outliers. *Computational statistics & data analysis* 47. 165-174.

[49]. Daya, A.A. (2015). Comparative study of C-A, C-P, and N-S fractal methods for separating geochemical anomalies from background: A case study of Kamoshgaran region, northwest of Iran. *Journal of Geochemical Exploration* 150. 52-63.

[50]. Chaturvedi, D., Satsangi, P. and Kalra, P. (1996). Effect of different mappings and normalization of neural network models, *Proceedings of the National Power Systems Conference*. Indian Institute of Technology, pp. 377-386.

[51]. Sola, J., Sevilla, J. (1997). Importance of input data normalization for the application of neural networks to complex industrial problems. *IEEE Transactions on Nuclear Science* 44. 1464-1468.

[52]. Demuth, H. and Beale, M. (1992). *Neural Network Toolbox. For Use with MATLAB*. The MathWorks Inc 2000.

- [53]. Kasiviswanathan, K., He, J., Sudheer, K. and Tay, J.-H. (2016). Potential application of wavelet neural network ensemble to forecast streamflow for flood management. *Journal of Hydrology* 536. 161-173.
- [54]. Crochemore, L., Perrin, C., Andréassian, V., Ehret, U., Seibert, S.P., Grimaldi, S., Gupta, H., Paturel, J.-E. (2015). Comparing expert judgement and numerical

criteria for hydrograph evaluation. *Hydrological Sciences Journal* 60. 402-423.

- [55]. Sreekanth, P., Geethanjali, N., Sreedevi, P., Ahmed, S., Kumar, N.R. and Jayanthi, P.K. (2009). Forecasting groundwater level using artificial neural networks. *Current science*. 933-939.

مشخص‌سازی زون‌های دگرسانی با روش‌های شبکه عصبی موجک (WNN) و فرکتال غلظت- حجم (C-V) در زون هیپوژن نهشته مس پورفیری، منطقه شهرباک، جنوب شرق ایران

بشیر شکوه سلجوقی* و اردشیر هزارخانی

بخش مهندسی معدن، دانشگاه صنعتی امیر کبیر تهران، ایران

ارسال ۲۰۲۰/۰۹/۱۸، پذیرش ۲۰۲۰/۱۰/۱۰

* نویسنده مسئول مکاتبات: bashir.shokouh@gmail.com

چکیده:

در این مقاله، ما قصد داریم به دو هدف خاص دست یابیم. نخستین هدف، بررسی قابلیت کاربرد تکنیک شبکه عصبی موجک (WNN) در تخمین عیار کانه است که مبتنی بر ترکیب نظریه موجک و شبکه عصبی مصنوعی (ANN) است. موجک‌های مختلف به عنوان توابع فعال‌سازی برای تخمین عیار مس داده‌های گمانه در زون هیپوژن نهشته پورفیری، ناحیه شهرباک، جنوب شرق ایران بکار برده شد. پارامترهای WNN مانند اتساع و انتقال ثابت بودند و تنها وزن‌های شبکه در طول فرایند یادگیری بهینه شدند. کارایی این نوع شبکه در یادگیری تابع و تخمین با روش کریجینگ معمولی (OK) مقایسه شد. دوم، ما قصد داریم تا نواحی دگرسانی پتاسیک و فیلیک را در زون هیپوژن نهشته مس پورفیری براساس تخمین بدست آمده از روش‌های WNN و OK و با استفاده از مدل فرکتال غلظت-حجم (C-V) مشخص نماییم. بدین منظور، در ابتدا نمودارهای لگاریتم-لگاریتم C-V براساس نتایج OK و WNN تولید شد. نمودارها سپس برای تعیین مقادیر آستانه مس زون‌های دگرسانی استفاده شدند. برای بررسی همبستگی بین مدل زمین‌شناسی و نتایج فرکتال C-V ماتریس لگاریتم ریشه‌ای بکار برده شد. نتایج نشان داد که مقادیر مس کمتر از ۱/۱ درصد روش WNN و کسل‌های همپوشان‌تری با زون دگرسانی فیلیک با صحت همپوشانی (OA) ۰/۷۴ دارد. همبستگی فضایی بین زون‌های دگرسانی پتاسیک مدلسازی زمین‌شناسی سه بعدی و زون‌های غلظت بالای در مدل فرکتال غلظت-حجم نشان داد که زون دگرسانی دارای مقادیر مس بین ۱/۱ درصد تا ۲/۲ درصد با OA حدود ۰/۷۲ است و در نهایت همپوشانی مناسبی با مقادیر مس بزرگتر از ۲/۲ درصد با OA حدود ۰/۷ دارد. به طور کلی، نتایج نشان داد که WNN با تابع فعال‌سازی مورلت با OA بزرگتر از OK می‌تواند ابزار مناسب و معتبرتری برای مدل‌سازی کمی زون‌های دگرسانی به‌جای روش‌های کیفی باشند.

کلمات کلیدی: زون‌های دگرسانی، کریجینگ معمولی (OK)، مدل فرکتال C-V، موجک، شبکه عصبی موجک (WNN)، شهرباک.